JPPIPA 8(6) (2022)

Jurnal Penelitian Pendidikan IPA

Journal of Research in Science Education

http://jppipa.unram.ac.id/index.php/jppipa/index

Deformation Analysis of 2012 Mw8.6 Indian Ocean Earthquake Based on GPS Data in Preseismic, Coseismic, and Postseismic Phases

Ikram Zul[1], Marzuki[1*], Vira Friska[1]

[1] Department of Physics, Universitas Andalas, Limau Manis, Padang 25163, Indonesa.

Received: November 10, 2022
Revised: December 17, 2022
Accepted: December 24, 2022
Published: December 31, 2022

Corresponding Author:
Marzuki
marzuki@sci.unand.ac.id

DOI: 10.29303/jppipa.v8i6.2419

Abstract: The earthquake was one of the biggest natural disasters in Sumatra and dramatically affected this region and the surrounding area. Determination of surface deformation due to the earthquake is essential for disaster mitigation. The Global Navigation Satellite System (GNSS) is a commonly used method for determining surface deformation due to earthquakes. This study analyzes surface deformation during the preseismic, coseismic, and postseismic phases due to the 2012 Mw8.6 Indian Ocean earthquake. The study used Global Positioning System (GPS) data from the Sumatran GPS Array (SuGAr) network. The most significant horizontal deformation was observed at the LEWK station, which was 280.554 mm towards the northeast and experienced a subsidence of 40.830 mm in vertical deformation. Horizontal deformation is still felt by 22.453 mm to the northeast and vertical deformation of 8.810 mm (uplift) at stations that are farther (580 km) from the earthquake's epicenter. However, in the observation period of 60 days (postseismic phase), stations closer to the epicenter are still experiencing a postseismic phase. In contrast, stations far from the epicenter show that the postseismic phase is almost complete. In the preseismic phase, all stations experience almost the same horizontal deformation, ranging from 2.210 mm-3.639 mm, but with a different direction of movement, which may be caused by previous intense earthquake activity, which is still releasing energy (postseismic phase). On the other hand, the vertical deformation during the preseismic phase generally experiences an uplift except at the LEWK station. The results of this study can be additional information for earthquake mitigation in the Sumatra region.

Keywords: SuGAr; Sumatra; surface deformation; 2012 Mw8.6 earthquake

Introduction

Sumatra has a high potential for large earthquakes due to plate movement activities around this region. Several plate activities in Sumatra are the subduction of the Indo-Australian Plate to the Eurasian Plate, which results in the formation of a subduction path (Hamzah et al., 2000; Prawirodirdjo et al., 2010). In addition, there is also an elongated fault that divides Sumatra in the right direction, known as the Sumatran Fault or Semangko Fault (Alif et al., 2020; McCaffrey, 1992), which has a velocity of 5 mm/year (Tong et al., 2018). In the Mentawai Islands, there is also a fault parallel to the Semangko Fault. This fault is a Backthrust with a southwesterly slope without strike-slip motion (Lori et al., 2018). Several major earthquakes in Sumatra include the 2004 Mw 9.2 Aceh-Andaman earthquake and the 2005 Mw8.6 Nias earthquake, were due to the subduction zone mechanism (Pollitz et al., 2012). The 2010 Mw7.8 Mentawai earthquake was one of the earthquakes caused by the Mentawai Backthrust activity (Marzuki et al., 2022). On April 11, 2012, there was also an earthquake with the magnitude of Mw8.6 in the Wharton Basin (west of the subduction zone), a plate boundary zone spreading between the Indian and Australian Plates. This earthquake was a strike-slip earthquake and is considered the largest strike-slip earthquake ever recorded (McGuire & Beroza, 2012; Meng et al., 2012).

How to Cite:
Marzuki, M., Ikram, Z., & Friska, V. (2022). Deformation Analysis of 2012 Mw8.6 Indian Ocean Earthquake Based on GPS Data in Preseismic, Coseismic, and Postseismic Phases. *Jurnal Penelitian Pendidikan IPA*, *8*(6), 2785–2792. https://doi.org/10.29303/jppipa.v8i6.2419

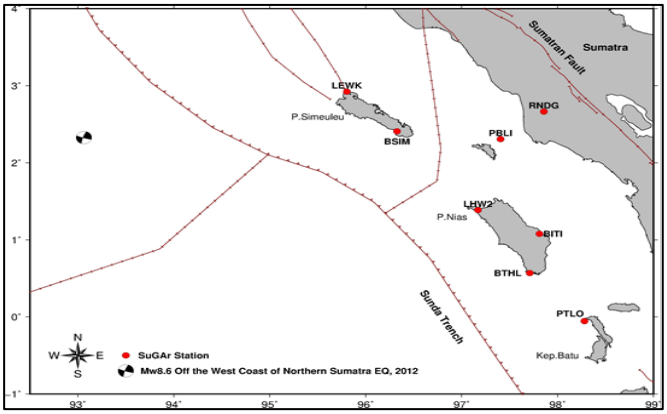

Figure 1. Distribution of SuGAr observation stations and epicenters of the 2012 Mw8.6 Indian Ocean earthquake.

Earthquakes will usually cause the surrounding earth's crust to deform in both horizontal and vertical directions. In an earthquake cycle, the deformation process can be divided into interseismic, praseismic, coseismic, and post-seismic phases/stages (Deputel et al., 2012; Natawidjaja et al., 2007). The interseismic stage is the initial stage of an earthquake cycle. At this stage, energy from within the earth moves the plates, and energy begins to accumulate in the parts of the plates where earthquakes usually occur (plate boundaries and faults). Just before the earthquake occurs, it is called the preseismic stage; when the main earthquake occurs, it is called the coseismic stage. Coseismic deformation is the deformation of the earth's crust caused by the main earthquake and its large aftershocks. This deformation is generally in the form of horizontal or vertical deformation, and its spatial scope is proportional to the earthquake's magnitude. The post-seismic stage is defined as the stage when the remnants of the earthquake energy are released slowly and over a long period until conditions return to a new equilibrium stage. Knowledge of deformation in each phase is needed in earthquake disaster mitigation.

This study analyzes the deformation caused by the 2012 Mw8.6 earthquake. Several studies have discussed this earthquake, and most studies address the slip model of the coseismic offset (Gunawan et al., 2016; Maulida et al., 2016; Pratama et al., 2018). Yadav et al. (2013) also performed coseismic offset calculations for the 2012 earthquake using GPS observations at stations generally located north of the earthquake epicenter. The results obtained are in the form of deformation at the station north of the earthquake epicenter, with values ranging from 17 mm-41 mm heading south. Stations in northern Sumatra show the direction of coseismic movement to the northwest, and stations located northwest of Sumatra experience movement to the northeast. Maulida et al. (2016) also calculated the deformation in the coseismic phase of the 2012 Mw8.6 Indian Ocean earthquake. They found deformation at the station on the northwest coast of Sumatra, heading northeast by ~30 cm, while in the central part of Sumatra, showing a deformation to the northwest of 3 cm. Vertically, they get a subsidence of 3 cm.

While there have been some studies on the 2012 Mw8.6 Indian Ocean earthquakes, such study has not discussed the deformations for all phases of the earthquake in detail. Therefore, we analyzed the deformation due to the 2012 earthquake for each preseismic phase, coseismic phase, and postseismic phase using Global Positioning System (GPS) station observation data. GPS is a navigation and positioning satellite system owned and managed by the United States. GPS data can record movements with submillimeter precision per year, and GPS has proven to be an indispensable tool in crustal deformation analysis (Khawiendratama, 2016) such as describing the conditions of observation points in all phases of the earthquake cycle (intereismic, preseismic, coseismic, and postseismic) (Catherine & Gahalaut, 2007; Govers et al., 2018). The GPS observations used in this study came from the SuGAr network (Sumatran GPS Array), eight stations located in the east-southeast of the earthquake epicenter. They were processed using GAMIT/GLOBK software. This research can be used to understand the characteristics of seismic activity and is expected to be used as stage information for earthquake mitigation in the affected area.

Method

Data

This study uses observational data from eight SuGAr stations located east-southeast of the 2012 earthquake epicenter (Table 1). SuGAr is a GPS station spread along the west coast of Sumatra Island (McLoughlin et al., 2011), extending for more than 1,000 km of convergent plate boundaries between the Indo-Australian and Asian Tectonic Plates. The distribution of SuGAr stations can be seen on the website sugar.geotek.lipi.go.id. SuGAr's data format is RINEX (Receiver Independent Exchange Format). The data used for this study are from the 072nd DOY (Day of Years) to the 162nd DOY in 2012, namely March 13-June 10, 2012 totaling 90 days. The preseismic phase is taken from data at DOY 072-100 and data for the postseismic phase, namely DOYs 104-162. In the coseismic phase, the data is from one day before the earthquake until one day after, namely DOY 101-103. RINEX SuGAr data can be downloaded through UNAVCO (University NAVSTAR Consortium), CDDIS (Crustal Dynamics Data Information System), and SOPAC (Scripps Orbit and Permanent Array)

Table 1. Location of SuGAr stations

Stations	Location	Longitude	Latitude	First Epoch	Last Epoch
BITI	Biouti, Nias	97.811371	1.07862	2012 03 13	2012 06 10
BSIM	Simeulue Airport	96.326157	2.40924	2012 03 13	2012 06 10
BTHL	Botohilithano	97.710701	0.56920	2012 03 13	2012 06 10
LEWK	Lewak	95.804077	2.92359	2012 03 13	2012 06 10
LHW2	Lahewa	97.171944	1.39688	2012 03 13	2012 06 10
PBLI	Balai Island	97.405296	2.30853	2012 03 13	2012 06 10
PTLO	Telo Island	98.280037	-0.05461	2012 03 13	2012 06 10
RNDG	Rundeng	97.857200	2.66524	2012 03 13	2012 06 10

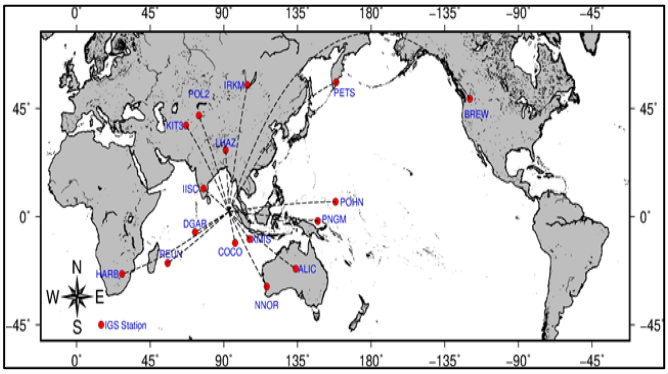

Figure 2. Distrubution of IGS stations used.

Another data used is data of IGS (International GNSS Service). The IGS is an international organization that is a collection of agencies around the world that collects permanent data sources from GNSS (Global Navigation Satellite System) stations and maintains GNSS stations (Johnston et al., 2017). IGS station information can be viewed on the igs network website, while the rinex IGS data can be downloaded using a command on Linux. The IGS station is used as a binding point, namely the point that binds the observation point, so that it can be seen that the observation point moves relative to the reference point. This study used 16 IGS stations spread out in all directions from the observation points. The location of the station can be seen in Figure 2. Besides IGS data, we also used navigational data and supporting data such as atmospheric modeling data, tidal modeling data, and weather modeling data.

Data processing

The RINEX data was processed using the GAMIT/GLOBK software in this study. GAMIT (GPS Analysis Massachusetts Institute of Technology) is an open-source software with a UNIX/LINUX-based platform. GAMIT is a package of tools for processing GPS data developed by the Massachusetts Institute of Technology (MIT) and the Scripps Institution of Oceanography (SIO), and Harvard University with support from the National Science Foundation (Herring et al., 2015). Data processing in GAMIT uses automatic batch processing by modifying the control file first. The control files in question are station.info files, lfile. files, sites.defaults files, sittbl. files, sittbl. files, and process.defaults files. Several files result from data processing using GAMIT software, including h-files containing adjustment values and variance-covariance matrices used as input in GLOBK processing, as well as q-files and summary files. In this study, the GAMIT version used is GAMIT 10.74.

GLOBK software creates time series by combining DOY and plotting coordinate parameters of h–files. The result of GLOBK processing is a file containing data on changes in the position of each station in topocentric coordinates (north, east, up) and geocentric coordinates (X, Y, Z). Furthermore, to determine the deformation, the position change data for each SuGAr station is calculated in a coordinate system using the equation:

$$\overrightarrow{dE} = \left(E - E_{reference}\right) x\ 111{,}320{,}000\ \text{mm} \quad (1)$$

$$\overrightarrow{dN} = \left(N - N_{reference}\right) x\ 111{,}320{,}000\ \text{mm} \quad (2)$$

$$\overrightarrow{dU} = \left(U - U_{reference}\right) x\ 1{,}000\ \text{mm} \quad (3)$$

where is $\overrightarrow{dE}$ magnitude of change in station position to the east, $\overrightarrow{dN}$ is magnitude of change in station position to the north, $\overrightarrow{dU}$ is magnitude of change in station position to the vertical, E is station position in the east direction, $E_{reference}$ is reference station position in the east direction, N is station position in the north direction, $N_{reference}$ is reference station position in the north direction, U is station position in the vertical direction, and $U_{reference}$ is reference station position in the vertical direction.

A linear regression equation is used to see the trend in the preseismic and postseismic phases. Furthermore, in the preseismic phase, the magnitude of the deformation to the north and the deformation to the east is calculated using the difference in the magnitude of the deformation at DOY 100 and DOY 73. In contrast, the postseismic phase is based on the difference in deformation at DOY 162 and DOY 103. The resultant and the deformation direction are calculated using equations (4) and (5).

$$\vec{R} = \sqrt{\left(\overrightarrow{dE}\right)^2 + \left(\overrightarrow{dN}\right)^2} \quad (4)$$

$$\alpha = arc\tan\frac{\overrightarrow{dE}}{\overrightarrow{dN}} \quad (5)$$

where $\vec{R}$ is resultant of SuGAr station deformation and α SuGAr station deformation direction.

The deformation vector of the SuGAr station was mapped using the GMT 5.4.5 software. The input of the map is the magnitude of the deformation in the east and north, and the vertical directions for each phase. Then an analysis was carried out on the deformation vectors of the preseismic, coseismic, and postseismic phases.

Result and Discussion

Time series of SuGAr station

The time series of the observation can be seen in Figure 3. The LEWK station is the closest to the earthquake epicenter (305 km), and the PTLO station is the farthest (580 km) from the earthquake epicenter. There is a significant coseismic jump difference between the two stations. The LEWK station has a clearer coseismic jump than the PTLO station because it is closer to the earthquake's epicenter. Before the earthquake, the two stations experienced a movement to the southwest. However, after the earthquake (postseismic phase), the direction changed to the northeast. The movement to the southwest in the preseismic phase is probably due to the postseismic phase of previous large earthquakes, such as the 2008 Simeulue earthquake and the 2010 Mentawai earthquake.

The slope trends in the preseismic and postseismic phases also differ between these two stations. At the LEWK station, the slope of the postseismic phase looks slightly different from the preseismic phase, whereas, at the PTLO station, the slope of the postseismic curve looks the same as the preseismic phase. This happens because the LEWK station, which is closer to the earthquake's epicenter, is still experiencing a postseismic phase during the observation period.

Preseismic Deformation

The preseismic phase is the phase before the earthquake. This study calculates the preseismic phase from DOY 073 to DOY 100 (~1 month). The magnitude of the horizontal and vertical deformations can be seen in Table 2 and Table 3. The horizontal deformation at the observation station is almost the same, ranging from 2.210 mm to 3.639 mm. When compared with the average speed of movement of the Indo-Australian Plate (subduction zone) of 60-70 mm/year (Natawidjaja et al., 2007), it is estimated that this velocity is ~5 mm/month. This preseismic deformation value is smaller than the monthly moving average and indicates an energy accumulation just before the earthquake (Xu et al., 2019).

Observation stations have various directions of movement. The direction of the horizontal movement of stations during the preseismic phase varies. BTHL, LEWK, LHW2, and PTLO stations experience a movement towards the northeast, which is consistent with the direction of the Indo-Australian Plate. In contrast, the BITI, BSIM, and PBLI stations point to the southeast. The RNDG station in mainland Sumatra experiences a movement towards the southwest. This is probably caused by the activity of the previous major earthquake, which is still experiencing a release of energy (postseismic phase). In the vertical direction, the amount of deformation in this phase has a variable value, but generally, the station has an uplift movement.

Cosesimic Deformation

Figure 5 shows the deformation direction of the observation station in the coseismic phase. Tables 2 and 3 show the horizontal and vertical deformation magnitude at each station. The horizontal deformation at each station is greater than in the preseismic and postseismic phases, a general characteristic of surface deformation (Arisa et al., 2021). The largest deformation value occurs at the LEWK station, followed by the BSIM and PBLI stations. These three stations have the shortest distance from the earthquake's epicenter compared to the other stations. All three experienced more than 100 mm deformation, while in the vertical direction, the LEWK station also experienced the greatest deformation compared to the other stations, namely, 40.830 mm. The magnitude of this horizontal and vertical deformation is consistent with that obtained by Maulida et al. (2016) and Yadav et al. (2013) in research on coseismic slip models using GPS data. Maulida et al. (2016) obtained deformation in the coseismic phase of ~30 cm to the northeast and deformation of ~5 cm in the vertical direction. Other stations also experience deformation in this phase. For example, the PTLO station, which was farthest from the earthquake's epicenter, was still affected by this earthquake, with a horizontal deformation of 22.453 mm and a vertical deformation of 2.471 mm.

Table 2. Magnitude of horizontal deformation during preseismic, coseismic, and postseismic phases.

Stations	Preseismic (mm)	Coseismic (mm)	Postseismic (mm)
BITI	2.210	51.723	10.022
BSIM	2.405	190.785	31.247
BTHL	3.115	34.024	8.749
LEWK	2.332	280.554	38.109
LHW2	3.070	77.223	14.575
PBLI	2.374	107.471	18.654
PTLO	3.639	22.453	5.693
RNDG	2.861	92.663	17.058

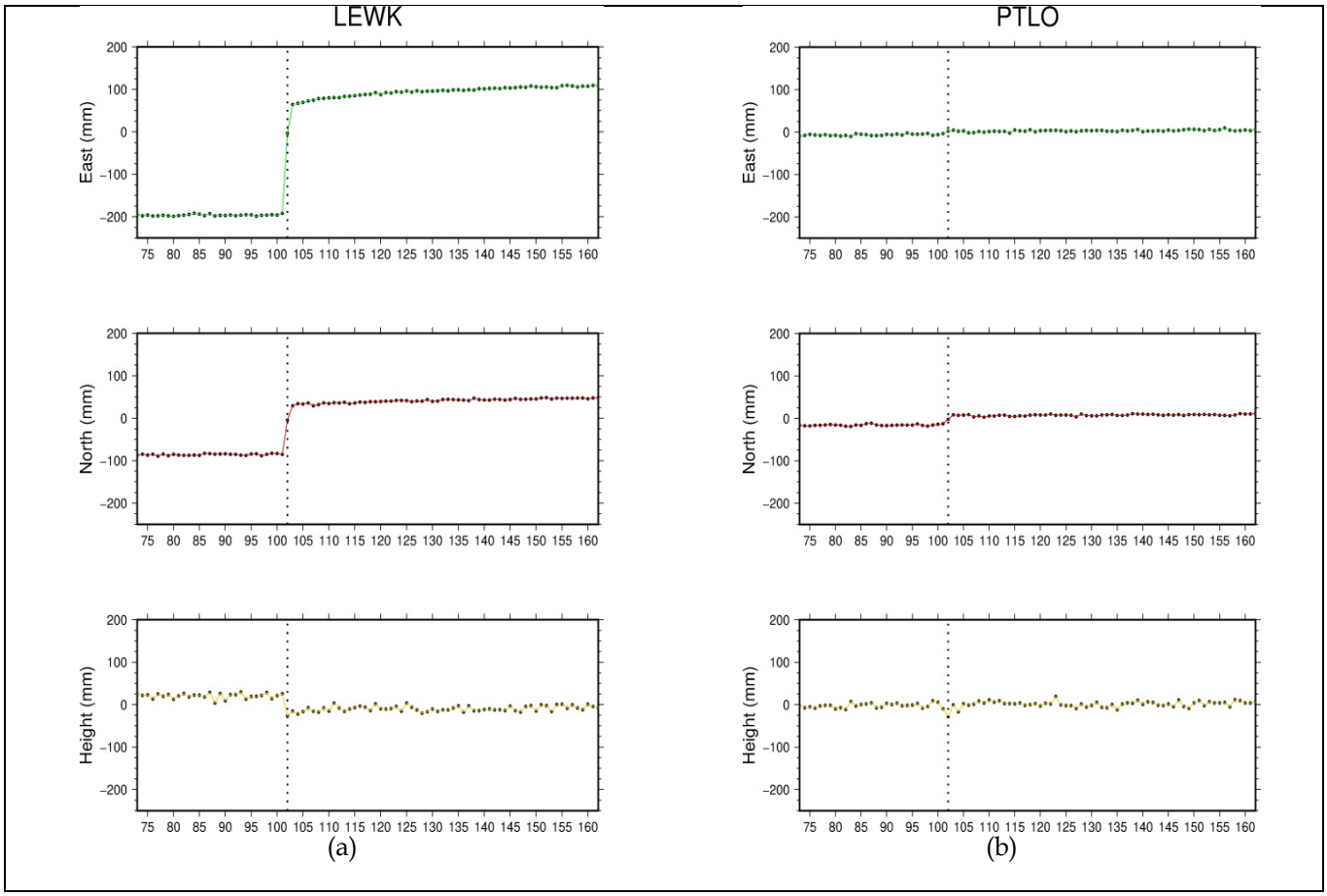

Figure 3. Time series of deformation at (a) LEWK and (b) PTLO stations. The *x*-axis is the observation time, and the *y*-axis is the position in the east-west (green curve), north-south (red curve), and up-down/up-down (yellow curve) directions. Coseismic jumps are marked with a black dotted line.

Table 3. Maginitude of vertical deformation during preseismic, coseismic, and postseismic phases.

Stations	Preseismic (mm)	Coseismic (mm)	Postseismic (mm)
BITI	1.863	-9.790	5.684
BSIM	0.270	-6.960	7.572
BTHL	7.641	13.960	5.632
LEWK	-0.856	-40.830	5.426
LHW2	14.120	4.350	-3.355
PBLI	2.357	20.000	11.351
PTLO	7.855	8.810	2.471
RNDG	8.795	-5.720	6.238

Table 4. Deformation direction during preseismic, coseismic, and postseismic phases.

Stations	Preseismic (°)	Coseismic (°)	Postseismic (°)
BITI	S38.57E	N22.34E	N10.68E
BSIM	S2.43E	N21.43E	N21.36E
BTHL	N9.86E	N47.32E	N36.04E
LEWK	N70.88E	N24.08E	N22.61E
LHW2	N3.53E	N25.75E	N17.82E
PBLI	S29.96E	N20.54E	N14.87E
PTLO	N20.45E	N69.27E	N38.36E
RNDG	S90.03W	N19.93E	N7.40E

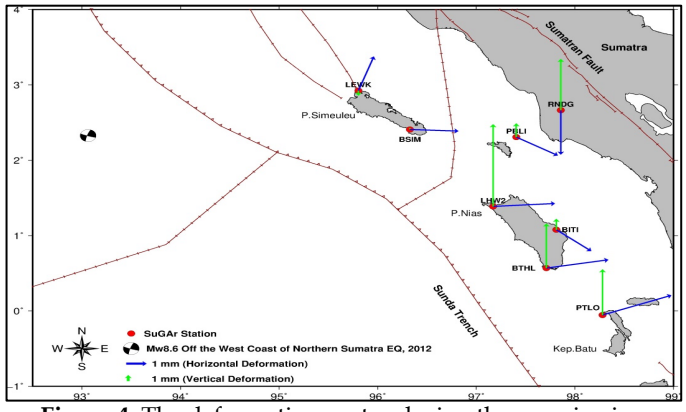

Figure 4. The deformation vector during the preseismic phase. A blue arrow indicates the horizontal preseismic deformation vector, and the vertical deformation vector is indicated by a green arrow with a scale of 1 mm.

All observation stations indicate the direction of movement to the northeast (Figure 5). The direction of this movement is the same as the movement of the Indo-Australian Plate. As explained earlier, the direction of deformation in this phase is opposite to that of the preseismic phase. This displacement is associated with a northwest-trending right-lateral fault (WNW) and a left-

lateral fault (NNE). Previous studies have shown that the WNW fault carries most of the slip (Duputel et al., 2012; Yue et al., 2012), while the NNE trending structure also has a larger slip (Satriano et al., 2012; Wei et al., 2013). Vertically, the previously described LEWK stations have decreased (subsidence). This indicates that the earthquake mechanism is not purely strike-slip (Maulida et al., 2016).

Vertical deformation in this phase has various directions. Some stations experienced subsidence, and others experienced an uplift. As explained by Natawidjaja et al. (2007), the number of islands will increase when an earthquake occurs. However, the subsidence that occurred at several stations could indicate that the mechanism of the earthquake was not a pure strike-slip earthquake.

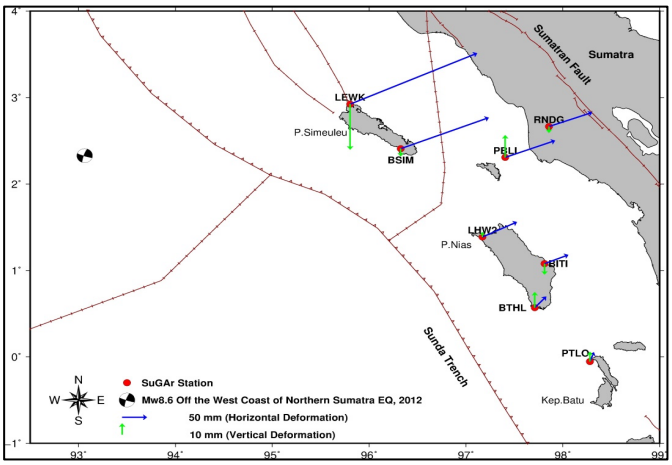

Figure 5. Vector deformation during the coseismic phase. Blue arrows indicate horizontal deformation with a scale of 50 mm. The green arrow indicates the vertical deformation with a scale of 10 mm.

Postseismic deformation

The magnitude of horizontal deformation in the postseismic phase is smaller than in the coseismic phase (Tables 2 and 3). In the postseismic phase, the remnants of earthquake energy are released slowly until conditions return to a new equilibrium state (Sajagat et al., 2016). The value of the deformation is still much different compared to the deformation in the preseismic phase, especially at the stations closest to the earthquake's epicenter. For example, at the LEWK station, the postseismic deformation of 38.109 mm is still much larger than the preseismic deformation of only 2.332 mm (Table 2). In contrast to the PTLO station, which is farthest from the earthquake epicenter, it has a postseismic deformation of 5.693 mm. This value is close to the preseismic deformation of 3.639 mm. Thus, during the observation period (DOY 104-DOY 162), the plate is still experiencing a postseismic phase characterized by values that are still much different from the preseismic phase. Similar to horizontal deformation, vertical deformation in this phase generally has a smaller value than in the coseismic phase.

Figure 6 shows the station's horizontal and vertical deformation vectors. The horizontal deformation in this phase is towards the northeast, the same as the deformation direction in the coseismic phase. However, based on the inclination angle, the station changes the direction of motion with the clockwise movement since the coseismic phase, which can be seen from a smaller angle than the coseismic phase. This movement is consistent with the movement of the Indo-Australian Plate, which has a clockwise movement (Mulyana, 2006). In vertical deformation, stations generally experience a change in direction from the coseismic phase. For example, at the BITI, BSIM, LEWK, and RNDG stations, which initially experienced subsidence during the coseismic phase, their motion changed to become uplift during the postseismic phase.

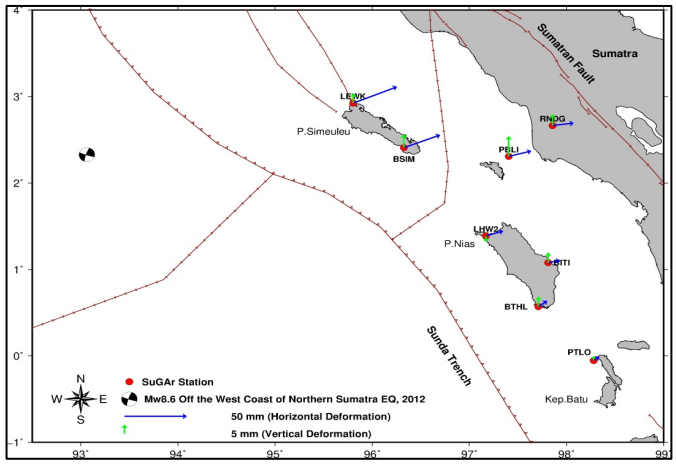

Figure 6. Deformation vector during the postseismic phase. Blue arrows indicate horizontal deformation with a scale of 50 mm, while green arrows with a scale of 5 mm indicate vertical deformation.

Conclusion

The results have shown differences in deformation during the preseismic, coseismic, and postseismic phases due to the 2012 Mw8.6 Indian Ocean Earthquake. During the preseismic phase, the largest horizontal deformation was observed at the LEWK station, which was 280.554 mm with a direction to the northeast. The vertical deformation showed a subsidence of 40.830 mm. During the postseismic phase (60 days), stations close to the epicenter still experience a postseismic phase, while stations far from the epicenter show values close to the preseismic phase indicating that the postseismic phase is almost complete. Finally, the results of this study also show that the earthquake mechanism is not purely strike-slip, consistent with several previous studies. The study results can strengthen the theory of the 2012 Mw8.6 Indian Ocean earthquake mechanism and be

additional information for Sumatra earthquake mitigation.

Acknowledgements

The present study was supported by KEMDIKBUD through the Penelitian Tesis Magister 2022 Scheme (Contract No.: 086/E5/PG.02.00.PT/2022). Furthermore, thanks to Geological Disaster Research Center, Earth Science and Maritime Research Organization, National Research and Innovation Agency (BRIN) and Nanyang Technological University's Earth Observatory of Singapore for operating the SuGAr network. Besides the GAMIT/GLOBK, the figures were plotted using GMT (General Mapping Tools).

References

Alif, S. M., Fattah, E. I., & Kholil, M. (2020). Geodetic slip rate and locking depth of east Semangko Fault derived from GPS measurement. *Geodesy and Geodynamics*, *11*(3), 222–228. https://doi.org/10.1016/j.geog.2020.04.002

Arisa, D., Setiadi, B., & Priyanto, W. S. (2021). Pre-and Coseismic Analysis of the Mw7.6 Padang Earthquake 2009 from Geodetic Approach. *IOP Conference Series: Earth and Environmental Science*, *789*(1). https://doi.org/10.1088/1755-1315/789/1/012069

Catherine, J. K., & Gahalaut, V. K. (2007). A glimpse of earthquake cycle in the Sumatra region. *Current Science, 92(1), 114–118*. Retrieved from https://www.jstor.org/stable/24096834

Duputel, Z., Kanamori, H., Tsai, V. C., Rivera, L., Meng, L., Ampuero, J. P., & Stock, J. M. (2012). The 2012 Sumatra great earthquake sequence. *Earth and Planetary Science Letters*, *351–352*, 247–257. https://doi.org/10.1016/j.epsl.2012.07.017

Govers, R., Furlong, K. P., van de Wiel, L., Herman, M. W., & Broerse, T. (2018). The Geodetic Signature of the Earthquake Cycle at Subduction Zones: Model Constraints on the Deep Processes. *Reviews of Geophysics*, *56*(1), 6–49. https://doi.org/10.1002/2017RG000586

Gunawan, E., Maulida, P., Meilano, I., Irsyam, M., & Efendi, J. (2016). Analysis of coseismic fault slip models of the 2012 Indian ocean earthquake: Importance of GPS data for crustal deformation studies. *Acta Geophysica*, *64*(6), 2136–2150. https://doi.org/10.1515/acgeo-2016-0106

Hamzah, L., Puspito, N., & Imamura, F. (2000). Tsunami Catalog Indonesia.pdf. In *Journal of Natural Disaster Science* (Vol. 22, Issue 1, pp. 25–43). Retrieved from https://www.jstage.jst.go.jp/article/jnds/22/1/22_1_25/_pdf

Herring, T. A., King, R. W., Floyd, M. A., & McClusky, S. C. (2015). GLOBK reference manual, version 10.6. *Massachusetts Institute of Technology: Cambridge, MA, USA*.

Johnston, G., Riddell, A., & Hausler, G. (2017). The International GNSS Service. *Springer Handbooks*, 967–982. https://doi.org/10.1007/978-3-319-42928-1_33

Khawiendratama, B. P. (2016). Analisa Perubahan Kecepatan Pergeseran Titik Akibat Gempa Menggunakan Data SuGar (Sumatran GPS Array). *Jurnal Teknik ITS*, *5*(2). https://doi.org/10.12962/j23373539.v5i2.17595

Lori Agung, S., Shandy, Y., Tri, U., & Fitri, A. (2018). Aktifitas Gempa Bumi Sumatera Barat Berdasarkan Sumber dari Januari hingga Juni 2018. *Stasiun Geofisika Kelas I Silaing Bawah*.

Marzuki, Ramadhan, R., Friska, V., Primadona, H., Ramadhan, R. A., Monica, F., Arisa, D., & Namigo, E. L. (2022). Dynamics of West Coast of Sumatra and Island Arc Mentawai during the Coseismic Phase of the Mentawai Mw7.8 25 October 2010 Earthquake. *Journal of Physics: Conference Series*, *2309*(1). https://doi.org/10.1088/1742-6596/2309/1/012030

Maulida, P., Meilano, I., Gunawan, E., & Efendi, J. (2016). Analysis of 2012 M8.6 Indian Ocean earthquake coseismic slip model based on GPS data. *AIP Conference Proceedings*, *1730*. https://doi.org/10.1063/1.4947396

McCaffrey, R. (1992). Oblique plate convergence, slip vectors, and forearc deformation. *Journal of Geophysical Research*, *97*(B6), 8905–8915. https://doi.org/10.1029/92JB00483

McGuire, J. J., & Beroza, G. C. (2012). A rogue earthquake off Sumatra. *Science*, *336*(6085), 1118–1119. https://doi.org/10.1126/science.1223983

McLoughlin, I. V., Wong, K. J., & Tan, S. L. (2011). Data collection, communications and processing in the Sumatran GPS array (SuGAr). *Proceedings of the World Congress on Engineering 2011, WCE 2011*, *2*, 1732–1736.

Meng, L., Ampuero, J. P., Stock, J., Duputel, Z., Luo, Y., & Tsai, V. C. (2012). Earthquake in a maze: Compressional rupture branching during the 2012 Mw 8.6 Sumatra earthquake. *Science*, *337*(6095), 724–726. https://doi.org/10.1126/science.1224030

Mulyana, B. (2006). Extension Tektonik Selat Sunda. *Bulletin of Scientific Contribution*, *6*(2), 137–145.

Natawidjaja, D. H., Sieh, K., Galetzka, J., Suwargadi, B. W., Cheng, H., Edwards, R. L., & Chlieh, M. (2007). Interseismic deformation above the Sunda Megathrust recorded in coral microatolls of the Mentawai islands, West Sumatra. *Journal of Geophysical Research: Solid Earth*, *112*(2), 1–27. https://doi.org/10.1029/2006JB004450

Pollitz, F. F., Stein, R. S., Sevilgen, V., & Bürgmann, R. (2012). The 11 April 2012 east Indian Ocean earthquake triggered large aftershocks worldwide. *Nature*, *490*(7419), 250–253. https://doi.org/10.1038/nature11504

Pratama, C., Ito, T., Tabei, T., Kimata, F., Gunawan, E., Ohta, Y., Yamashina, T., Nurdin, I., Sugiyanto, D., Muksin, U., Ismail, N., & Meilano, I. (2018). Evaluation of the 2012 Indian Ocean coseismic fault model in 3-D heterogeneous structure based on vertical and horizontal GNSS observation. *AIP Conference Proceedings*, *1987*. https://doi.org/10.1063/1.5047296

Prawirodirdjo, L., McCaffrey, R., Chadwell, C. D., Bock, Y., & Subarya, C. (2010). Geodetic observations of an earthquake cycle at the Sumatra subduction zone: Role of interseismic strain segmentation. *Journal of Geophysical Research: Solid Earth*, *115*(3), 1–15. https://doi.org/10.1029/2008JB006139

Sajagat, M. J., Awaluddin, M., & Yuwono, B. D. (2016). Hitungan Kecepatan Pergerakan Stasiun Sugar Akibat Proses Interseismik Gempa Mentawai 2007. *Jurnal Geodesi Undip*, *5*(4), 196–206. Retrieved from https://ejournal3.undip.ac.id/index.php/geodesi/article/view/13938

Satriano, C., Kiraly, E., Bernard, P., & Vilotte, J. P. (2012). The 2012 Mw 8.6 Sumatra earthquake: Evidence of westward sequential seismic ruptures associated to the reactivation of a N-S ocean fabric. *Geophysical Research Letters*, *39*(15), 1–6. https://doi.org/10.1029/2012GL052387

Tong, X., Sandwell, D. T., & Schmidt, D. A. (2018). Surface Creep Rate and Moment Accumulation Rate Along the Aceh Segment of the Sumatran Fault From L-band ALOS-1/PALSAR-1 Observations. *Geophysical Research Letters*, *45*(8), 3404–3412. https://doi.org/10.1002/2017GL076723

Wei, S., Helmberger, D., & Avouac, J. P. (2013). Modeling the 2012 Wharton basin earthquakes off-Sumatra: Complete lithospheric failure. *Journal of Geophysical Research: Solid Earth*, *118*(7), 3592–3609. https://doi.org/10.1002/jgrb.50267

Xu, K., Gan, W., & Wu, J. (2019). Pre-seismic deformation detected from regional GNSS observation network: A case study of the 2013 Lushan, eastern Tibetan Plateau (China), Ms 7.0 earthquake. *Journal of Asian Earth Sciences*, *180*(May), 103859. https://doi.org/10.1016/j.jseaes.2019.05.004

Yadav, R. K., Kundu, B., Gahalaut, K., Catherine, J., Gahalaut, V. K., Ambikapthy, A., & Naidu, M. S. (2013). Coseismic offsets due to the 11 April 2012 Indian Ocean earthquakes (M w 8.6 and 8.2) derived from GPS measurements. *Geophysical Research Letters*, *40*(13), 3389–3393. https://doi.org/10.1002/grl.50601

Yue, H., Lay, T., & Koper, K. D. (2012). En échelon and orthogonal fault ruptures of the 11 April 2012 great intraplate earthquakes. *Nature*, *490*(7419), 245–249. https://doi.org/10.1038/nature11492